ANTIOXIDANTS & REDOX SIGNALING
Volume 6, Number 3, 2004

Forum Review

In Vivo Spin Trapping of Nitric Oxide

LAWRENCE J. BERLINER[1] and HIROTADA FUJII[2]

ABSTRACT

The measurement of nitric oxide (NO) in biological samples has normally required destructive chemical techniques. The ability to detect NO non-invasively in living animals or excised organs has great potential using specialized electron paramagnetic resonance (EPR) methods. Although NO is paramagnetic, it cannot be observed directly unless it is complexed with ferrous iron-dithiocarbamate ligand spin trap complexes. Despite the minimally invasive nature of the technique, highly sensitive localized concentrations of NO may be observed ("trapped") *in vivo* by both L-band EPR and magnetic resonance imaging. *Antioxid. Redox Signal.* 6, 649–656.

INTRODUCTION

IN ORDER TO UNDERSTAND how nitric oxide (NO) is biosynthesized in tissues and how it mediates various physiological responses, it would be desirable to observe at the site of NO production. While several methods of analyzing NO exist, including chemiluminescence, oxyhemoglobin, gas chromatography–mass spectrometry, chemical measurements of NO_2^-/NO_3^-, fluorescent dye, and nitrosyl-hemoglobin formation by electron paramagnetic resonance (EPR) (14–16, 22, 35, 36), none of these methods can be applied non-invasively to experimental animals *in vivo* in real time.

INDIRECT DETECTION OF NO BY EPR

There are two classes of NO detection by EPR: "Indirect" detection involves observing the EPR of some other compound that is directly affected by reaction with NO; the "direct" method is where the NO is part of a specific ligand complex, and the NO is directly observed by EPR. EPR measurement of hemoglobin-bound NO has been used in the past (10). This is normally done with excised blood or tissue samples. The most optimal conditions are at liquid nitrogen temperature (which is obviously unsuitable for *in vivo* work). In addition, the maximum sensitivity is not as good as the dithiocarbamate "spin traps," which are discussed later.

There are several other, yet somewhat "indirect," EPR methods available. One involves the use of *N*-oxide "spin labels," one of which also has the properties of a spin trap. A class, the imidazolineoxy-*N*-oxides, is available in the form of 2-phenyl-4,4,5,5-tetramethylimidazole-1-oxy-3-oxide(PTIO) or the carboxy derivative or its ester, carboxymethoxy-PTIO (1, 37). The imidazolineoxyl-*N*-oxides react with rate constants of the order of $10^4\ M^{-1}\ s^{-1}$ with concomitant generation of NO_2^-/NO_3^-. This was also demonstrated *in vivo* by an apparent inhibition of vasorelaxant effectiveness by virtue of the depletion of NO levels (1). The nitronyl and nitroxyl radicals of the iminonitroxide type trap NO as monitored by the appearance of additional ^{14}N super-hyperfine structure from the new adduct (37). The distinctive change in hyperfine structure allows one to monitor the increase in a new narrow line component. On the other hand, the multiline hyperfine structure comes at the price of decreased peak height. A major problem with nitroxide/nitroxyl radicals, however, is their susceptibility to rapid bioreduction to the diamagnetic hydroxylamine, which is a problem that usually cannot be circumvented.

DIRECT DETECTION OF NO BY EPR

The use of dithiocarbamate:Fe(II) complexes was pioneered by the group of Kubrina and co-workers (17, 25) using

[1]Department of Chemistry and Biochemistry, University of Denver, Denver, CO.
[2]School of Health Sciences, Sapporo Medical University, Sapporo, Hokkaido, Japan.

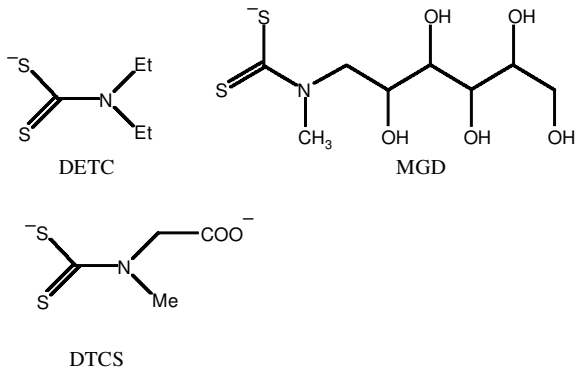

FIG. 1. Dithiocarbamate spin traps.

N,N-diethyldithiocarbamate (DETC) in the form of the $(DETC)_2$-Fe(II) complex, and then shortly thereafter by Lai and Komarov (21) and Komarov and Lai (15) using the water-soluble *N*-methyl-D-glucamine dithiocarbamate (MGD) as the corresponding $(MGD)_2$-Fe(II) complex. Another water-soluble reagent reported later was (dithiocarboxy)sarcosine (DTCS) as the corresponding $(DTCS)_2$-Fe(II) complex (39). Their structures are shown in Fig. 1. Each of these "spin traps" shows high affinity for NO. The EPR spectrum of, *e.g.*, low-spin $(MGD)_2$-Fe(II)-NO complex yields a characteristic three-line spectrum of a_N = 12.5 G and g_{iso} = 2.04, typical of an unpaired electron interacting with a (I = 1) ^{14}N nucleus. What is special about these traps is that there are no contributions from soluble or gaseous NO or from the diamagnetic $(MGD)_2$-Fe(II) complex. The sensitivity at L-band (1 GHz) for an *in vivo* "object" falls in the low micromolar NO concentrations. In order to maximize the sensitivity, high concentrations of the iron-dithiocarbamate ligands are employed. Other factors that would also enter into the absolute sensitivity are the stability of the NO complex at the particular site where it is generated. The reagents are inexpensive and commercially available and appear to be non-toxic at the levels typically used *in vivo* [100 m*M* dithiocarbamate, 20 m*M* Fe(II)]. Even while the dithiocarbamate "spin traps" are the most optimal reagents in use today, the principal shortcoming is still concentration sensitivity, which limits studies to pathological or disease states of elevated NO and/or NO synthase (NOS) levels.

Due to solubility differences of the various NO trapping reagents in water, hydrophobic $(DETC)_2$-Fe(II) and hydrophilic $(MGD)_2$-Fe(II) must be administered differently in animals. When $(DETC)_2$-Fe(II) is formed by mixing DETC with Fe(II) sulfate, it precipitates in aqueous media. Therefore, DETC and/or iron sulfate solutions must be injected (intraperitoneally or intramuscularly) separately. In the case of $(MGD)_2$-Fe(II), which is soluble in aqueous media, the complex can be injected directly into the animal.

Throughout this paper we distinguish between two types of "*in vivo*" EPR measurements. In one method the animal is subjected to injections of dithiocarbamate spin trap complex and then subsequently sacrificed for organ/tissue excision. Then *ex vivo* EPR is measured at X-band in flat quartz tissue cells. The advantage here is the increased sensitivity at levels that would be otherwise undetectable at L-band. The other method, L-band *in vivo* EPR, is whole-animal localized spectroscopy or imaging. The obvious advantage of experimenting on a live whole animal carries the tradeoff of lower sensitivity.

MONITORING NO IN THE BRAIN—*EX VIVO* EXPERIMENTS

Figure 2 depicts X-band EPR spectra of several liver and brain tissue samples from septic-shock rats induced by lipopolysaccharide (LPS). Typical triple-line EPR spectra of the $(DETC)_2$-Fe(II)-NO complex (a_N = 12.8 G, g = 2.04) are detected in liver and brain tissue (cerebellum, cortex, and hippocampus), where the estimated concentrations of NO were 79.5 ± 11.8, 11.6 ± 0.9, 8.3 ± 1.1, and 17.0 ± 1.5 nmol/g of tissue, respectively. Note that the olfactory bulb was essentially *devoid* of detectable NO (8). Similar levels were observed in excised heart (14.6 ± 1.5 nmol/g of tissue, n = 3), blood (1.2 ± 0.24 nmol/g of blood, n = 3), and kidney (3.5 ± 1.1 nmol/g of tissue, n = 3).

NO trapping studies have been done using both $(MGD)_2$-Fe(II) and $(DETC)_2$-Fe(II) under the same conditions (Fig. 3). The EPR signal intensities with $(MGD)_2$-Fe(II)-NO were almost the same in the liver (74.3 ± 10.3 nmol/g of tissue, n = 3) as found with $(DETC)_2$-Fe(II) (79.5 ± 11.8 nmol/g of tissue, n = 3). However, no $(MGD)_2$-Fe(II)-NO was detected

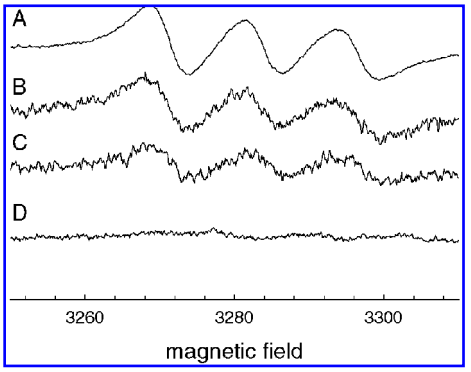

FIG. 2. X-band EPR spectra of $(DETC)_2$-Fe(II)-NO in excised tissues after *in vivo* administration of LPS, DETC, and ferrous sulfate: (A) liver (receiver gain; 5 × reduction), (B) hippocampus, (C) cerebellum, and (D) olfactory bulb. Rats were injected intraperitoneally with LPS (50 mg/kg) in saline, and after 6 h DETC (500 mg/kg) was injected intraperitoneally followed by subcutaneous injection of a mixture of ferrous sulfate (100 mg/kg) and sodium citrate (500 mg/kg). Finally, 1 h after the final injection, rats were sacrificed under anesthesia, and each tissue was immediately excised and either kept on dry ice until EPR measurement or measured immediately. Controls without LPS showed very-low-intensity EPR spectra. While several concentrations of each trapping reagent were tested, 100 mg/kg of ferrous sulfate was most optimal for efficient NO trapping. Typical spectrometer conditions were: microwave power, 20 mW; 100 kHz modulation amplitude, 1.0 G; sweep rate, 50 G/min; response time, 0.3 s. Reproduced from Fujii and Berliner (7) with permission.

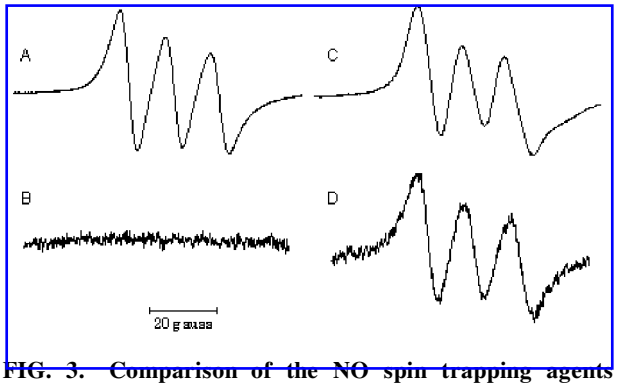

FIG. 3. Comparison of the NO spin trapping agents $(DETC)_2$-Fe(II) and $(MGD)_2$-Fe(II) in LPS-induced rats: EPR spectra of $(MGD)_2$-Fe(II)-NO in liver (A) and brain (B) and $(DETC)_2$-Fe(II)-NO in liver (C) and brain (D). LPS, DETC, and ferrous sulfate were adminstered as described in the legend of Fig. 2. An aliquot of $(MGD)_2$-Fe(II) spin trapping solution (MGD, 100 m*M*; $FeSO_4$, 20 m*M*) was subcutaneously injected 6 h after LPS injection. All other conditions were identical to those in Fig. 2. Reproduced from Fujii and Berliner (7) with permission.

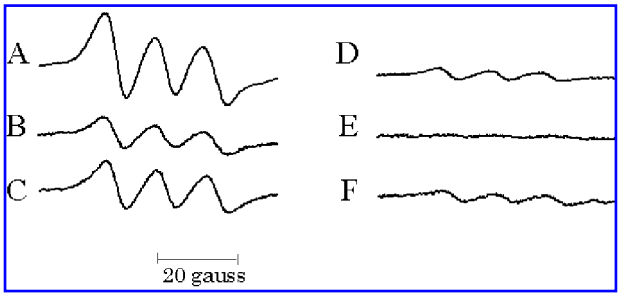

FIG. 4. Inhibitory effect of L-NMMA on NO generation in LPS-treated rats. X-band EPR spectra were measured in excised tissues from LPS-induced rats: without L-NMMA, liver (**A**), cerebellum (**B**), and heart (**C**); with ^{1}-NMMA, liver (**D**), cerebellum (**E**), and heart (**F**). Spectral intensities of A and D are shown as 50% reductions. Injection of LPS, DETC, and ferrous sulfate was carried out as described in the legend of Fig. 2 with and without L-NMMA (50 mg/kg in saline), administered intraperitoneally 3 h after LPS injection. As a control, saline solutions containing no L-NMMA were injected. All other conditions were identical to those in Fig. 2. Reproduced from Fujii and Berliner (7) with permission.

in the brain of septic-shock rats (Fig. 3B), although distinct EPR signals of $(DETC)_2$-Fe(II)-NO were observed (Fig. 3D) when hydrophobic $(DETC)_2$-Fe(II) was used. The concentration of $(DETC)_2$-Fe(II)-NO complex found in the brain was almost 20% of that in the liver. These results suggest that the NO observed in the brain was generated by NOS within brain tissue, *not* from blood or tissue surrounding the brain. This conclusion is supported by organ distribution studies where preformed $(MGD)_2$-Fe(II)-NO complex was injected via the tail vein of rats and fairly strong EPR signals were detected in the liver, heart, and blood, but not in the brain, again confirming that $(MGD)_2$-Fe(II)-NO formed in the veins, not brain tissue. On the other hand, the potential route for the lipophilic DETC is to cross the blood–brain barrier and then complex with tissue Fe(II), subsequently followed by NO generation within the brain tissue.

NON-ENZYMATIC GENERATION OF NO

NO can be generated in biological systems either enzymatically by NOS or via various non-enzymatic mechanisms. It is important to establish that NO detected in an LPS-induced septic-shock animal is generated enzymatically instead of by simple chemical reduction of nitrite/nitrate. In order to distinguish whether NO is produced enzymatically or not, one employs a competitive inhibitor for NOS, such as *N*-monomethyl-L-arginine (L-NMMA). As shown in Fig. 4, NO levels in the brain, heart, and liver of septic-shock rats were suppressed significantly in the presence of L-NMMA (down to 10–20% of the control), confirming that NOS was the source of NO. Several other examples of non-enzymatic NO pathways have been reported (11). In a very special case, Morez *et al.* (26) showed that NO might even originate from the breakdown of NOS inhibitors, such as L-NMMA. They used another NOS inhibitor, 3-bromo-7-indazole, that specifically inhibits brain neuronal NOS and induced NOS (iNOS) by an entirely different mechanism (3). Although not shown in Fig. 4, 3-bromo-7-indazole inhibited NO generation in the brain of animals as detected by EPR with the $(DETC)_2$-Fe(II)-NO complex, similar to that observed with L-NMMA. Consequently, the dithiocarbamate-iron-NO EPR signal originates from NOS (7). As a double check, it is important to measure the nitrite/nitrate levels in these same tissues to verify that they are significantly less than the NO concentrations measured by EPR. Another experiment, shown later in Fig. 5d, utilizes ^{15}N-L-arginine as a substrate to show that ^{15}NO is produced.

SUPPRESSION OF iNOS EXPRESSION BY PBN

The spin trap phenyl-*N*-*tert*-butyl nitrone (PBN) suppresses the induction of iNOS in the liver of LPS-treated mice (23). One possible suggested mechanism was blocking the expression of iNOS mRNA by inactivating nuclear factor κB transcription factor, preventing the overproduction of NO and a reduction in endotoxin-mediated death. In order to show this effect *in vivo* as monitored by NO production, we carried out EPR experiments in LPS-induced mice, which were pretreated and post-treated with PBN (Fig. 5). When PBN was injected either 30 min before or 2 h after LPS administration, the EPR signals shown in Fig. 5b and c were observed. Since PBN inhibits iNOS expression (23), the $(MGD)_2$-Fe(II)-NO signal was significantly suppressed when PBN was added *before* LPS administration (Fig. 5b). However, when PBN was added *after* LPS administration, *i.e.,* after iNOS expression was initiated, the resultant signal intensity (Fig. 5c) was similar to the control (Fig. 5a). Figure 6 depicts spectra using the lipophilic $(DETC)_2$-Fe(II)-NO complex to detect NO in the brain of LPS-induced rats.

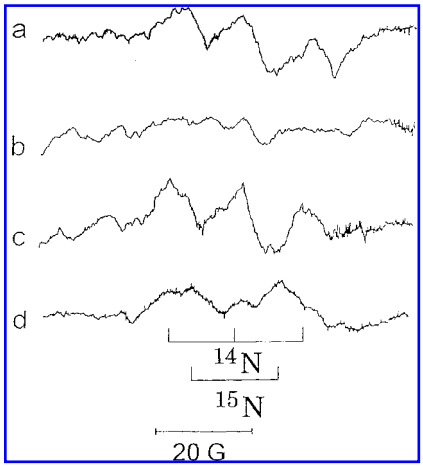

FIG. 5. ***In vivo*** **L-band EPR spectra of $(MGD)_2$-Fe(II)-NO in LPS-treated mice. a:** An approximately 20-g mouse was injected intraperitoneally with LPS in saline (1 mg/0.3 ml), and after 6 h injected subcutaneously with 0.4 ml of $(MGD)_2$-Fe(II) complex in saline [MGD:Fe(II), 100 m*M*:20 m*M*]. After 2 h following the last injection the *in vivo* EPR spectrum was measured. **b:** Same as (a), except that PBN (6 mg/0.5 ml of saline) was injected intraperitoneally into the mouse 30 min *before* LPS administration. **c:** Same as (a), except that the PBN was injected intraperitoneally 2 h *after* LPS administration. **d:** Same as (a), except that ^{15}N-L-arginine (10 mg/0.3 ml of saline) was injected intraperitoneally into the mouse 6 h after LPS administration, and just prior to the injection of the $(MGD)_2$-Fe(II) complex. Spectrometer conditions were as follows: frequency, 1.25 GHz; applied magnetic field, 425 G; incident microwave power, 50 mW; 20 kHz modulation amplitude, 1.0 G; sweep rate, 50 G/min; response time, 0.3 s. Reproduced from Fujii *et al.* (8) with permission.

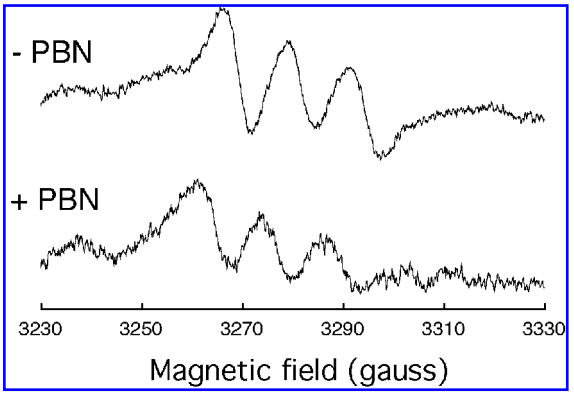

FIG. 6. Effects of PBN on NO generation in LPS-treated rats. X-band EPR spectra were measured in cerebellum brain tissue excised from LPS-induced rats. Rats were injected with LPS, DETC, and ferrous sulfate as described in the legend of Fig. 3. PBN (250 mg/kg) was administered intraperitoneally in rats 30 min before LPS injection. Saline solutions containing no PBN were injected as a control. All other conditions were identical to those in Fig. 3.

Remarkably, NO levels were *not* in the brain, although PBN is well known to cross the blood–brain barrier (26). Note that NO generation was suppressed (>80%) in the liver and heart, where high levels of iNOS are normally expressed (data not shown). The marked difference in PBN effects in the brain could be due to different iNOS species, mRNA, or its transcription mechanism versus liver (13). Alternatively, there are reports that a profound induction of iNOS mRNA in vascular, glial, and neuronal structures occurs (38).

IN VIVO SPIN TRAPPING OF NO

The first *in vivo* NO detection was reported by Lai and Komarov (21) and Komarov and Lai (15) at S-band. They detected $(MGD)_2$-Fe(II)-NO in endotoxin-shocked mice, but the studies were limited to the tail as this was the only non-lossy region body tissue at this frequency (3 GHz). On the other hand, direct localization of NO in mice is not restricted to any region with L-band *in vivo* spectrometers. Quaresima *et al.* (29) were able to detect NO at L-band in the liver of septic-shock mice using $(DETC)_2$-Fe(II) as the spin trap. Due mainly to spectrometer sensitivity limitations, a low signal-to-noise, yet detectable, $(DETC)_2$-Fe(II)-NO signal was observed with a characteristic three-line EPR spectrum (a_N = 13.04 G, g_{iso} = 2.04) at ambient temperature. Yoshimura *et al.* (39) used the NO spin trap DTCS to measure endogenous NO generation in the mouse abdomen at 700 MHz.

Fujii *et al.* (8) ran control experiments with preformed $(MGD)_2$-Fe(II)-NO complex in order to assess its pharmacological distribution in animals. $(MGD)_2$-Fe(II)-NO levels in the liver were very high yet undetectable in the brain. It was found at relatively low levels (3–5 μ*M*) in the head region, *i.e.,* the complex was distributed only in the blood *surrounding* the brain since $(MGD)_2$-Fe(II)-NO cannot pass the blood–brain barrier.

NO levels from constitutive NOS are found typically at picomolar levels (27, 28). In contrast, intracellular iNOS activity stimulated by endotoxin exposure can remain elevated for several hours, producing micromolar concentrations of NO (31–33), and the extent is dependent on LPS dose (24). This was also reflected in the EPR results, where at optimal LPS levels for iNOS induction (50 mg/kg), a strong L-band EPR spectrum was obtained from the upper abdomen (such as shown in Fig. 5a) that compared well with that of $(MGD)_2$-Fe(II)-NO control in saline.

The EPR signal intensities of $(MGD)_2$-Fe(II)-NO was surveyed from "head to toe," and the strongest signals were only detected near the upper abdomen. The mice were then sacrificed in order to determine pharmacological distributions of this complex, and the amount of NO complex was measured *ex vivo* at X-band as summarized in Table 1. Among all of the organs screened, the maximum NO levels were again in the liver (63.0 ± 10.3 nmol/g), which was at least five times larger than that found in the kidney, 11.5 ± 2.3 nmol/g (Table 1). These data are very consistent with other biological data suggesting that iNOS is expressed mainly in the liver by LPS induction.

The direct *in vivo* EPR observation of NO generation in the brain has recently been demonstrated with rodent models of

TABLE 1. QUANTITATION OF $(MGD)_2$-FE(II)-NO PRODUCED IN VARIOUS ORGANS BY *EX VIVO* EPR

Organ	*$(MGD)_2$-Fe(II)-NO (nmol/g of tissue)* (n = *3*)
Liver	63.0 ± 10.3
Kidney	11.5 ± 2.3
Blood (tail)	5.3 ± 1.4
Urine	9.7 ± 2.1

The amounts of $(MGD)_2$-Fe(II)-NO complex presented are mean ± SEM. Reproduced from Fujii *et al.* (8) with permission.

epileptic seizure (12). The role of NO in epileptogenesis was studied by a chemically induced seizure model using pentylenetetrazole (PTZ). NO generation was measured directly in the brain of a PTZ-induced mouse *in vivo* in an L-band EPR spectrometer. An elevation in NO production in the brain was observed during convulsions, and more NO was generated in tonic versus clonic seizures as shown in Fig. 7. This was the first report of direct *in vivo* observation of NO in the brain by EPR.

HIGH-RESOLUTION VISUALIZATION OF *IN VIVO* NO GENERATION: MAGNETIC RESONANCE IMAGING SPIN TRAPPING

The *in vivo* EPR results, combined with pharmacodistribution data, show that NO is produced mainly in the upper abdomen near the liver (8). However, a detailed visualization of NO distribution by EPR imaging would be most desirable. Yoshimura *et al.* (39), using *in vivo* EPR imaging of NO with the $(DTCS)_2$-Fe(II) spin trap, visualized the abdominal region of an LPS-pretreated mouse. The crescent-shaped image was just over the right abdomen of the mouse, with the outline corresponding anatomically to the liver. In addition, Suzuki *et al.* (34) obtained two-dimensional *in vivo* EPR images in live mice produced from the nitrovasodilator isosorbide dinitrate. In a higher-resolution *ex vivo* experiment, Kuppusamy *et al.* (19, 20) showed three-dimensional images in excised rat brain. The right hemisphere of the brain was subjected to ischemia-hypoxia, removed, and frozen in liquid nitrogen. *Ex vivo* EPR imaging with frozen organs might be more practical for detecting two- or three-dimensional distributions of bioradicals during extreme biological events in order to visualize superoxide and lipoxy radicals. Hence, although several groups have demonstrated the feasibility of imaging free radical distributions *in vivo* (6, 18, 20, 34, 39, 40), the spatial resolution of most EPR imaging spectrometers is not satisfactory enough to resolve much fine structure in organs for most free radicals, especially when the intrinsic linewidths are large, such as is the case with spin-trapped NO. $(MGD)_2$-Fe(II)-NO complex has a 3.5 G linewidth, which is a principal contributor to poor image resolution.

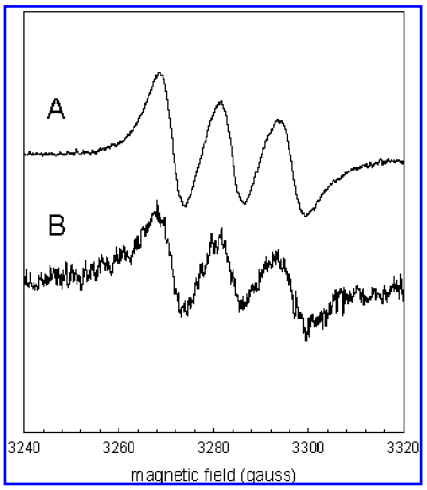

FIG. 7. *In vivo* L-band EPR spectra of $(DETC)_2$-Fe(II)-NO complex in mice doped with PTZ. DETC and iron were injected identically to that described in the legend of Fig. 2, 30 min before PTZ administration. **A:** Mice were doped with PTZ at a dose of 80 mg/kg. After tonic convulsions were observed, the mice were immediately anesthetized by pentobarbital (35 mg/kg) and measured by *in vivo* EPR spectroscopy. **B:** Same as A, except that mice were doped with PTZ at a dose of 40 mg/kg. These animals experienced clonic convulsions. Spectrometer conditions were identical with those in Fig. 5.

The alternative approach is the combination of magnetic resonance imaging (MRI) with EPR as first demonstrated by Brasch *et al.* (4), who used paramagnetic nitroxyl radicals as MRI contrast agents for enhancement of renal structures in animal models. Several other groups then reported experiments utilizing a range of nitroxides as contrast agents and their versatility in image enhancement (5, 30). Yet, while nitroxides function as contrast agents, they have major shortcomings since their biological half-lives are frequently too short to use in practice. On the other hand, would iron-dithiocarbamate-NO complexes work as contrast agents?

The reduction/decomposition of the NO-dithiocarbamate-iron complexes in the presence of 1 m*M* ascorbic acid or glutathione occurs with a half-life of about 40.2 ± 4.6 and 48.4 ± 5.2 min, respectively, which is much better than most nitroxides. $(MGD)_2$-Fe(II)-NO complexes show remarkably strong proton relaxation enhancement. The T_1 relaxivity at 20 and 85 MHz was found to be 0.31 and 0.27 mM^{-1} s^{-1}, respectively, and the T_2 relaxivity was 0.31 and 0.35 mM^{-1} s^{-1}, respectively (9). The relaxivity was also not very frequency dependent over this range, similar to that found with nitroxides (2, 5, 30). The T_1 relaxivity of the uncomplexed $(MGD)_2$-Fe(II) "spin trap" was 0.044 mM^{-1} s^{-1} at both 20 and 85 MHz, which is negligible, as are free Fe(II) and uncomplexed NO. Thus, the distinct increase in relaxivity occurs only after complexing NO with $(MGD)_2$-Fe(II), *i.e.,* it should be feasible to visualize the region *in vivo* where the NO was trapped as exploited in enhanced signal intensity in T_1- or T_2-weighted MR images.

Figure 8 shows T_1-weighted MR images of rats in a region near the liver before and after injection of the preformed $(MGD)_2$-Fe(II)-NO complex. Intraperitoneal injection (2 ml of 9.1 m*M* solution) directly into rats resulted in image enhancement of several tissues, clearly demonstrating that the NO complex is a very effective NO-specific contrast agent. The relative signal intensity was increased as much as 3.2 ±

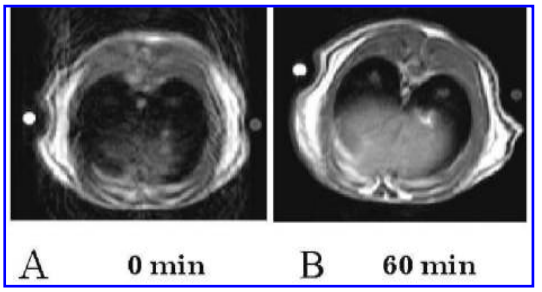

FIG. 8. T_1-weighted MR images in the axial plane of the liver of Wistar rats: (A) control, before injection of $(MGD)_2$ Fe(II)-NO; and (B) 60 min after injection of $(MGD)_2$-Fe(II)-NO complex. Two millliliters of 9.5 m*M* $(MGD)_2$-Fe(II)-NO complex, made from NO gas and $(MGD)_2$-Fe(II), was injected intraperitoneally at the lower abdomen of rats (250 g). Reproduced from Fujii *et al.* (9) with permission.

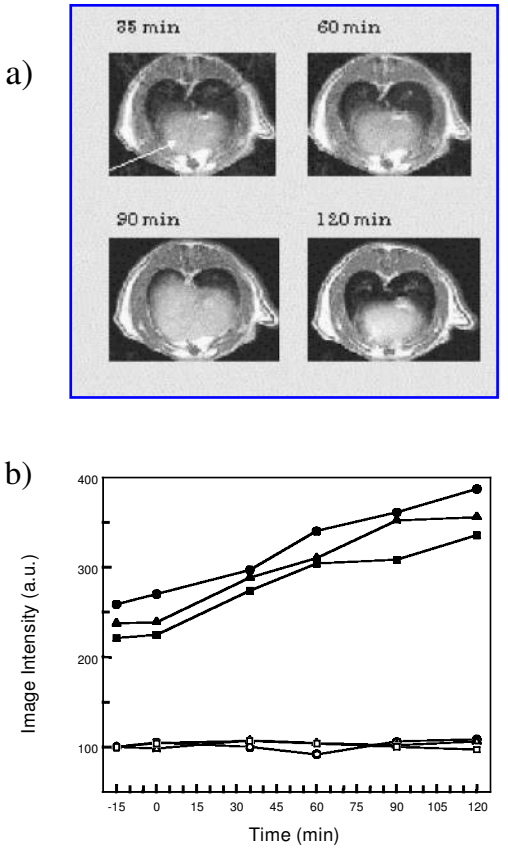

FIG. 9. Imaging of NO in LPS-treated rats. a: Transverse T_1-weighted MR images focused on a selected region of the liver in LPS-doped rats. The MR images were measured at the times indicated. Six hours after LPS injection, the NO spin trap [3 ml of $(MGD)_2$-Fe(II)] (MGD, 100 m*M*; Fe, 20 m*M*) was administered intraperitoneally. **b:** Plot of MR image intensity with time. Signal intensities were averaged over the selected region indicated by the arrow in a 7 × 7 mm^2 area for three different animals (filled symbols), normalized to intensity of a reference (water in a tube placed next to the animal, open symbols). At zero-time, the spin-trap $(MGD)_2$-Fe(II) was added. a.u., arbitrary units. Reproduced from Fujii *et al.* (9) with permission.

0.3 times (n = 3) in selected regions of the liver (estimated by EPR to be 150 ± 52 nmol/g of tissue from excised liver from the same rat).

In order to test the efficacy of this method during a real pathological event, rats were examined after induction of septic shock. At 6 h after LPS administration, the rats were injected intraperitoneally with $(MGD)_2$-Fe(II) and subsequently measured by MRI. Figure 9 shows the time dependence of MR images of septic-shock rats at different times after administration of $(MGD)_2$-Fe(II). The liver was clearly distinct from other organs, and the image intensity increased with time (Fig. 9), reaching a maximum at 90–120 min after spin trap injection for the slice shown. This time dependence was consistent with published EPR results showing that the signal intensity maximized at 90–120 min (8). In order to show that this NO generation was indeed from NOS, MRI experiments were carried out where the inhibitor L-NMMA was administered 3 h after LPS injection. As shown in Fig. 10, the image enhancement was suppressed after inhibiting NOS with L-NMMA. This methodology has been coined *MRI spin trapping,* which is not only suitable for mapping NO, but is also be valid for other important free radicals *in vivo* when combined with appropriate spin-trapping reagent techniques.

CONCLUSIONS AND PERSPECTIVES

In vivo EPR applications to NO-related problems have already been demonstrated to be quite promising and informative. The advent of MRI spin trapping for monitoring NO opens up the possibilities of imaging both large animals or humans at high resolution. The future potential for specifically targeted NO detection lies in the synthesis of appropriate "affinity label" dithiocarbamate compounds.

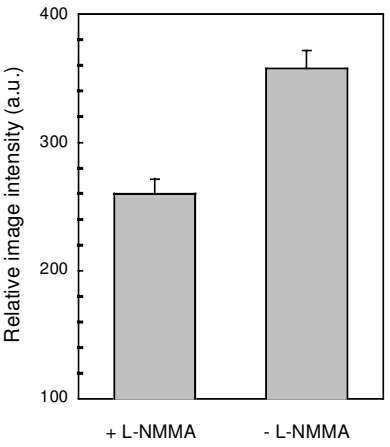

FIG. 10. Comparison of the signal intensity in the selected slice region of the liver in the presence and absence of the NOS inhibitor L-NMMA. The image intensity in the liver was first normalized to the intensity of a reference (water in the tube placed next to the animal). The normalized intensity in the selected regions (same as Fig. 9, 7 × 7 mm^2) was averaged. L-NMMA (50 mg/kg in saline) was intraperitoneally injected 3 h after LPS injection. a.u., arbitrary units. Reproduced from Fujii *et al.* (9) with permission.

ABBREVIATIONS

DETC, *N,N*-diethyldithiocarbamate; DTCS, (dithiocarboxy)sarcosine; EPR, electron paramagnetic resonance; iNOS, induced nitric oxide synthase; LPS, lipopolysaccharide; MGD, *N*-methyl-D-glucamine dithiocarbamate; MR, magnetic resonance; MRI, magnetic resonance imaging; NO, nitric oxide; NOS, nitric oxide synthase; PBN, phenyl *N-tert*-butyl nitrone; PTIO, 2-phenyl-4,4,5,5-tetramethylimidazole-1-oxy-3-oxide; PTZ, pentylenetetrazole.

REFERENCES

1. Akaike T, Yoshida M, Miyamoto Y, Sato K, Kohno M, Sasamoto K, Miyazaki K, Ueda S, and Maeda H. Antagonistic action of imidazolineoxyl N-oxides against endothelium-derived relaxing factor/NO through a radical reaction. *Biochemistry* 32: 827–832, 1993.
2. Bennett HF, Brown RD III, Keana JF, Koenig SH, and Swartz HM. Interactions of nitroxides with plasma and blood: effect on $1/T_1$ of water protons. *Magn Reson Med* 14: 40–55, 1990.
3. Bland-Ward PA and Moore PK. 7-Nitro indazole derivatives are potent inhibitors of brain, endothelium and inducible isoforms of nitric oxide synthase. *Life Sci* 57: 131–135, 1995.
4. Brasch RC, London DA, Wesbey GE, Tozer TN, Nitecki DE, Williams RD, Doemeny J, Tuck LD, and Lallemand DP. Work in progress: nuclear magnetic resonance study of a paramagnetic nitroxide contrast agent for enhancement of renal structures in experimental animals. *Radiology* 147: 773–779, 1983.
5. Chen HC, Sun KQ, Magin RL, and Swartz HM. Potential of albumin labeled with nitroxides as a contrast agent for magnetic resonance imaging and spectroscopy. *Bioconjug Chem* 1: 32–36, 1990.
6. Fujii H and Berliner LJ. One- and two-dimensional EPR imaging studies on phantoms and plant specimens. *Magn Reson Med* 2: 275–282, 1985.
7. Fujii H and Berliner LJ. Ex-vivo detection of nitric oxide in brain tissue. *Magn Reson Med* 42: 599–602, 1999.
8. Fujii H, Koscielniak J, and Berliner LJ. Determination and characterization of nitric oxide generation in mice by in-vivo L-band EPR spectroscopy. *Magn Reson Med* 38: 565–568, 1997.
9. Fujii H, Wan X, Zhong J, Berliner LJ, and Yoshikawa K. *In vivo* imaging of spin-trapped nitric oxide in rats with septic shock: MRI spin trapping. *Magn Reson Med* 42: 235–239, 1999.
10. Hille R, Olson JS, and Palmer G. Spectral transitions of nitrosyl hemes during ligand binding to hemoglobin. *J Biol Chem* 254: 12110–12120, 1979.
11. Hiramoto K, Tomiyama S, and Kikugawa K. Appearance of electron spin resonance signals in the interaction of dithiocarbamate-Fe(II) with nitrogen dioxide and nitrite. *Free Radic Res* 27: 505–509, 1997
12. Kaneko K, Itoh K, Berliner LJ, Miyasaka K, and Fujii H. Consequences of nitric oxide generation in epileptic-seizure rodent models as studied by *in vivo* EPR. *Magn Reson Med* 48: 1051–1056, 2002.
13. Knowles RG, Merrett M, Salter M, and Moncada S. Differential induction of brain, lung and liver nitric oxide synthase by endotoxin in the rat. *Biochem J* 270: 833–836, 1990.
14. Kojima H, Sakurai K, Kikuchi K, Kawahara S, Kirino Y, Nagoshi H, Hirata Y, and Nagano T. Development of a fluorescent indicator for nitric oxide based on the fluorescein chromophore. *Chem Pharm Bull* 46: 373–375, 1998.
15. Komarov A and Lai CS. Detection of nitric oxide production in mice by spin trapping electron paramagnetic resonance spectroscopy. *Biochim Biophys Acta* 1272: 29–36, 1995.
16. Kosaka H, Watanabe M, Yoshihara H, Harada N, and Shiga T. Detection of nitric oxide production in lipopolysaccharide-treated rats by ESR using carbon monoxide hemoglobin. *Biochem Biophys Res Commun* 184: 1119–1124, 1992.
17. Kubrina LN, Mikoyan VD, Mordvintcev PI, and Vanin AF. EPR evidence for nitric oxide production from guanidino nitrogens of L-arginine. *Biochim Biophys Acta* 1176: 140–144, 1993.
18. Kuppusamy P, Chzhan M, Vij K, Shteynbuk M, Lefer D, Giannella E, and Zweier JL. Three-dimensional spectral-spatial EPR imaging of free radicals in the heart: a technique for imaging tissue metabolism and oxygenation. *Proc Natl Acad Sci U S A* 91: 3388–3392, 1994.
19. Kuppusamy P, Ohnishi ST, Numagami Y, Ohnishi T, and Zweier JL. Three-dimensional imaging of nitric oxide production in the rat brain subjected to ischemia-hypoxia. *J Cereb Blood Flow Metab* 15: 899–903, 1995.
20. Kuppusamy P, Wang P, Samouilov A, and Zweier JL. Spatial mapping of nitric oxide generation in the ischemic heart using electron paramagnetic resonance imaging. *Magn Reson Med* 36: 212–218, 1996.
21. Lai CS and Komarov A. Spin trapping of nitric oxide produced in-vivo in septic-shock mice. *FEBS Lett* 345: 120–124, 1994.
22. Lancaster JR Jr, Langrehr JM, Bergonia HA, Murase N, Simmons RL, and Hoffman RA. EPR detection of heme and nonheme iron-containing protein nitrosylation by nitric oxide during rejection of rat heart allograft. *J Biol Chem* 184: 1119–1124, 1992.
23. Miyajima T and Kotake Y. Spin trapping agent, phenyl N tert-butyl nitrone, inhibits induction of nitric oxide synthase in endotoxin-induced shock in mice. *Biochem Biophys Res Commun* 215: 114–121, 1995.
24. Moncada S, Palmer RMJ, and Higgs EA. Nitric oxide: physiology, pathophysiology, and pharmacology. *Pharmacol Rev* 43: 109–142, 1991.
25. Mordvintcev P, Mulsch A, Busse R, and Vanin A. On-line detection of nitric oxide formation in liquid aqueous phase by electron paramagnetic resonance spectroscopy. *Anal Biochem* 199: 142–146, 1991.
26. Morez LL, Norby SW, Cruz L, Sweedler JV, Gillette R, and Clarkson RB. Non-enzymatic production of nitric oxide (NO) from NO synthase inhibitors. *Biochem Biophys Res Commun* 253: 571–576, 1998.
27. Nathan CF. Nitric oxide as a secretory product of mammalian cells. *FASEB J* 6: 3051–3064, 1992.

28. Palmer RM, Rees DD, Ashton DS, and Moncada S. L-arginine is the physiological precursor for the formation of nitric oxide in endothelium-dependent relaxation. *Biochem Biophys Res Commun* 153: 1251–1256, 1988.
29. Quaresima V, Takehara H, Tsushima K, Ferrari M, and Utsumi H. *In vivo* detection of mouse liver nitric oxide generation by spin trapping electron paramagnetic resonance spectroscopy. *Biochem Biophys Res Commun* 221: 729–734, 1996.
30. Slane JM, Lai CS, and Hyde JS. A proton relaxation enhancement investigation of the binding of fatty acid spin labels to human serum albumin. *Magn Reson Med* 3: 699–706, 1986.
31. Stuehr DJ and Griffith OW. Mammalian nitric oxide synthases. *Adv Enzymol Relat Areas Mol Biol* 65: 287–346, 1992.
32. Stuehr DJ and Marletta MA. Induction of nitrite/nitrate synthesis in murine macrophages by BCG infection, lymphokines, or interferon gamma. *J Immunol* 139: 518–527, 1987.
33. Stuehr DJ, Kwon NS, Nathan CF, Griffith OW, Feldmann PL, and Wiseman J. N omega-hydroxyl-L-arginine is an intermediate in the biosynthesis of nitric oxide from L-arginine. *J Biol Chem* 266: 6259–6263, 1991.
34. Suzuki Y, Fujii S, Numagami Y, Tominaga T, Yoshimoto T, and Yoshimura T. In vivo nitric oxide detection in the septic rat brain by electron paramagnetic resonance. *Free Radic Res* 28: 293–299, 1998.
35. Wang QZ, Jacobs J, DeLeo J, Kruszyna H, Kruszyna R, Smith R, and Wilcox D. Nitric oxide hemoglobin in mice and rats in endotoxic shock. *Life Sci* 49: 55–60, 1991.
36. Westenberger U, Thanner S, Ruf HH, Gersonde K, Sutter G, and Trentz O. Formation of free radicals and nitric oxide derivative of hemoglobin in rats during shock syndrome. *Free Radic Res Commun* 11: 167–178, 1990.
37. Woldman YY, Khramtsov VV, Grigor'ev IA, Kirilju IA, and Utepbergenov DI. Spin trapping of nitric oxide by nitronylnitroxides: measurement of the activity of NO synthase from rat cerebellum. *Biochem Biophys Res Commun* 202: 195–203, 1994.
38. Wong M-L, Rettori V, Al-Shekhlee A, Bongiorno PB, and Canteros G. Inducible nitric oxide synthase gene expression in the brain during systemic inflammation. *Nat Med* 2: 581–584, 1996.
39. Yoshimura T, Yokoyama H, Fujii S, Takeyama F, Oikawa K, and Kamada H. *In vivo* EPR detection and imaging of endogenous nitric oxide in lipopolysaccharide-treated mice. *Nat Biotechnol* 14: 992–994, 1996.
40. Zweier J, Wang P, and Kuppusamy P. Direct measurement of nitric oxide generation in the ischemic heart using electron paramagnetic resonance spectroscopy. *J Biol Chem* 270: 304–307, 1995.

Address reprint requests to:
Lawrence J. Berliner
Professor and Chair
Department of Chemistry & Biochemistry
University of Denver
2190 East Iliff Avenue
F.W. Olin Hall, Room 202
Denver, CO 80208–2436

E-mail: berliner@du.edu

Received for publication July 17, 2003; accepted February 19, 2004.

This article has been cited by:

1. Ivan Spasojevi#. 2011. Free radicals and antioxidants at a glance using EPR spectroscopy. *Critical Reviews in Clinical Laboratory Sciences* **48**:3, 114-142. [CrossRef]
2. Marek Ziaja, Jolanta Lubieniecka, Michalina Lewicka, Janusz Pyka, Przemyslaw M. Plonka. 2011. Changes in nitric oxide content following injury to the neonatal rat brain. *Brain Research* **1367**, 319-329. [CrossRef]
3. Ivan Spasojevi#. 2010. Electron Paramagnetic Resonance - A Powerful Tool of Medical Biochemistry in Discovering Mechanisms of Disease and Treatment Prospects. *Journal of Medical Biochemistry* **29**:3, 175-188. [CrossRef]
4. Ana Nemec, Zlatko Pavlica, Milan Petelin, David A. Crossley, Marjeta Šentjurc, Aleš Jerin, Damijan Eržen, Irena Zdovc, Tina Hitti, Uroš Skaleri#. 2010. Systemic use of selective iNOS inhibitor 1400W or non-selective NOS inhibitor l-NAME differently affects systemic nitric oxide formation after oral Porphyromonas gingivalis inoculation in mice. *Archives of Oral Biology* **55**:7, 509-514. [CrossRef]
5. Hao Hong, Jiangtao Sun, Weibo Cai. 2009. Multimodality imaging of nitric oxide and nitric oxide synthases. *Free Radical Biology and Medicine* **47**:6, 684-698. [CrossRef]
6. A. Nemec, Z. Pavlica, D. A. Crossley, M. Šentjurc, A. Jerin, D. Eržen, M. Vrecl, G. Majdi#, I. Zdovc, M. Petelin, U. Skaleri#. 2009. Chronic ingestion of Porphyromonas gingivalis induces systemic nitric oxide response in mice. *Oral Microbiology and Immunology* **24**:3, 204-210. [CrossRef]
7. Pierre Sonveaux, Bénédicte F. Jordan, Bernard Gallez, Olivier Feron. 2009. Nitric oxide delivery to cancer: Why and how?. *European Journal of Cancer* **45**:8, 1352-1369. [CrossRef]
8. Andrea Bernini, Vincenzo Venditti, Ottavia Spiga, Neri Niccolai. 2009. Probing protein surface accessibility with solvent and paramagnetic molecules. *Progress in Nuclear Magnetic Resonance Spectroscopy* **54**:3-4, 278-289. [CrossRef]
9. Ana Nemec, Zlatko Pavlica, David A. Crossley, Irena Zdovc, Damijan Eržen, Marjeta Šentjurc, Marjana Nemec, Milan Petelin. 2009. Single oral inoculation with Escherichia coli (ATCC 25922) stimulates generalised production of nitric oxide in mice. *Acta Veterinaria Hungarica* **57**:1, 127-138. [CrossRef]
10. A. Nemec, Z. Pavlica, M. Šentjurc, D. A. Crossley, A. Jerin, D. Eržen, I. Zdovc, M. Petelin, U. Skaleri#. 2008. Single gavage with Porphyromonas gingivalis reduces acute systemic nitric oxide response in mice. *Oral Microbiology and Immunology* **23**:5, 435-439. [CrossRef]
11. Ernst E. van Faassen, Maarten P. Koeners, Jaap A. Joles, Anatoly F. Vanin. 2008. Detection of basal NO production in rat tissues using iron–dithiocarbamate complexes. *Nitric Oxide* **18**:4, 279-286. [CrossRef]
12. Marek Ziaja , Janusz Pyka , Anna Machowska , Anna Maslanka , Przemyslaw M. Plonka . 2007. Nitric Oxide Spin-Trapping and NADPH-Diaphorase Activity in Mature Rat Brain after Injury. *Journal of Neurotrauma* **24**:12, 1845-1854. [Abstract] [Full Text PDF] [Full Text PDF with Links]
13. Harold M. Swartz , Nadeem Khan , Valery V. Khramtsov . 2007. Use of Electron Paramagnetic Resonance Spectroscopy to Evaluate the Redox State In Vivo. *Antioxidants & Redox Signaling* **9**:10, 1757-1772. [Abstract] [Full Text PDF] [Full Text PDF with Links]
14. A KLESCHYOV, P WENZEL, T MUNZEL. 2007. Electron paramagnetic resonance (EPR) spin trapping of biological nitric oxide#. *Journal of Chromatography B* **851**:1-2, 12-20. [CrossRef]
15. Susannah Renew, Eiri Heyno, Peter Schopfer, Anja Liszkay. 2005. Sensitive detection and localization of hydroxyl radical production in cucumber roots and Arabidopsis seedlings by spin trapping electron paramagnetic resonance spectroscopy. *The Plant Journal* **44**:2, 342-347. [CrossRef]
16. John Weaver, Supatra Porasuphatana, Pei Tsai, Theodore Budzichowski, Gerald M. Rosen. 2005. Spin trapping nitric oxide from neuronal nitric oxide synthase: A look at several iron–dithiocarbamate complexes. *Free Radical Research* **39**:10, 1027-1033. [CrossRef]

17. Periannan Kuppusamy . 2004. EPR Spectroscopy in Biology and Medicine. *Antioxidants & Redox Signaling* **6**:3, 583-585. [Citation] [Full Text PDF] [Full Text PDF with Links]